Effect of quantum well thickness and temperature on electrical and optical characteristics of transistor laser using group-IV material

Jaspinder Kaur[1] · Rikmantra Basu[2] · Ajay Kumar Sharma[1]

Abstract
Group IV $Ge_{1-x}Sn_x$ alloy in bulk form and heterostructures using quantum wells (QWs) GeSn/SiGeSn pairs show promise for laser sources in recent years. In this paper, we present the design of transistor laser (TL) structure with a SiGeSn emitter, GeSn QW embedded in the SiGeSn base, and a GeSn collector grown on the top of 200 nm thick strain-relaxed GeSn buffer, compatible with current CMOS technology. The GeSn layer is assumed to have composition of $x > 0.08$ to achieve the direct band-gap nature. The lasing is examined in terms of minimum base threshold current and optimum lasing action obtained by using $Ge_{0.87}Sn_{0.13}/Si_{0.05}Ge_{0.82}Sn_{0.13}$ MQW TL structure. The performance of proposed structure is compared with the theoretical values of already reported GeSn TL and some of the experimental values of InGaAs TL. The proposed design reduces the lasing threshold base current to some extent (~ 1.133 mA) and enhances the modulation bandwidth upto ~ 75.9 GHz.

Keywords Group IV photonics · (Si)GeSn · Multi quantum wells · Threshold base current · Modulation bandwidth

1 Introduction

Currently, the increasing demand of inter and intra-chip data throughput necessitates the modifications in the current CMOS technology ensuring the enhancement of bandwidth and reduction in power consumption (Miller 2000). With the electronic and photonic

---

✉ Jaspinder Kaur
  jaspinderkaur@nitdelhi.ac.in

  Rikmantra Basu
  rikmantrabasu@nitdelhi.ac.in

  Ajay Kumar Sharma
  drsharmaajayk@gmail.com

1   Department of Computer Science and Engineering, National Institute of Technology Delhi, Narela, Delhi 110040, India

2   Department of Electronics and Communication Engineering, National Institute of Technology Delhi, Narela, Delhi 110040, India

circuit integration on silicon (Si) platform, it would be possible to fulfill such requirements (Stange et al. 2018). Transistor laser (TLs) is an electronic device that can function as a transistor giving optical as well as electrical output simultaneously. It was first demonstrated by Feng and co-workers in 2004 (Feng et al. 2004a). Since then, a number of research groups reported theoretical and experimental characteristics of TLs by using different materials, especially group III–V compounds, and their metallurgy (Basu et al. 2015a). The literature also contain a number of research articles discussing the TL model in detail (Faraji et al. 2009; Taghavi et al. 2012; Basu et al. 2011, 2013, 2012a, b). (Basu et al. 2011, 2013, 2012a, b) considered a more general analytical model for TL that uses continuity equations, virtual states (VS) to account for electron transfer from 3 to 2D in QW subbands, and Fermi's golden rule to calculate gain in QWs by using density-of-states and level broadening for 2D QWs. According to all of these papers, the estimated values of threshold base current, laser light output power and injected carrier profile in the base region agreed well with the reported experimental values. The TLs based on Group III–V semiconductors shows excellent performance but they suffered from some limitations including maturity problems, lack of integration, high cost, toxicity in nature etc.

Additionally, the indirect bandgap of Group IV semiconductors such as Si, Ge, and their alloys make them unsuitable for optoelectronic and photonic devices. However, the situation has changed dramatically in recent years, thanks to the unstrained and strained growth, both succeed GeSn alloy on virtual substrates. It is found that with the increase of Sn (tin) concentration, the Γ valley drops faster than the conduction band of L valley, changing GeSn into a direct-bandgap semiconductor for Sn content of 8% and above (Chang et al. 2010; Ranjan and Das 2016). It is because of the direct nature of the bandgap that workers are developing various photonic devices on Si platform. So, GeSn based heterophototransistors (Chang et al. 2016; Basu et al. 2015b; Pandey et al. 2018), optically pumped lasers (Wirths et al. 2015), PIN and APD photodetectors (Oheme and Al 2012; Hossain et al. 2017) have been reported so far.

This paper investigate the lasing properties of $Ge_{0.87}Sn_{0.13}/Si_{0.05}Ge_{0.82}Sn_{0.13}$ MQW TL with GeSn QWs in the base and SiGeSn barriers. This is due to the fact that Ge is not a suitable barrier material to confine the carriers in the GeSn well. By contrast, using ternary alloys such as SiGeSn, electrons and holes can be constrained simultaneously. We chose to use a moderately high Sn concentration of 13% in the active layer (Stange et al. 2018). In order to obtain modified expressions for terminal currents, we first select any position of the QW in the base. Considering the subband energies and envelope functions in the presence of strain, the density of state function in 2D, polarization-dependent momentum matrix elements, Fermi distribution, and lineshape functions, the gain in the QW is obtained. Our study comprises the investigation of MQW $Ge_{0.87}Sn_{0.13}/Si_{0.05}Ge_{0.82}Sn_{0.13}$ TL with different well thicknesses and at different temperatures and comparison in accordance with already values reported by GeSn TL (Basu et al. 2019; Mukhopadhyay et al. 2018) and some of the experimental and theoretical values of InGaAs TL (Feng et al. 2004b, 2007, 2006; Then et al. 2010) in terms of threshold base current, emitted light output power and modulation bandwidth. Moreover, comparing our proposed structure to already reported InGaAs TL and GeSn TL values, we find a significant reduction in threshold base current and, at the same time, an increase in light output power at different temperatures. Higher modulation bandwidth is also predicted.

In Sect. 2, we describe the GeSn TL structure. Section 3 provides the relevant expressions and material parameters. In Sect. 4, we discuss the results along with their implications, and in Sect. 5, we draw conclusions.
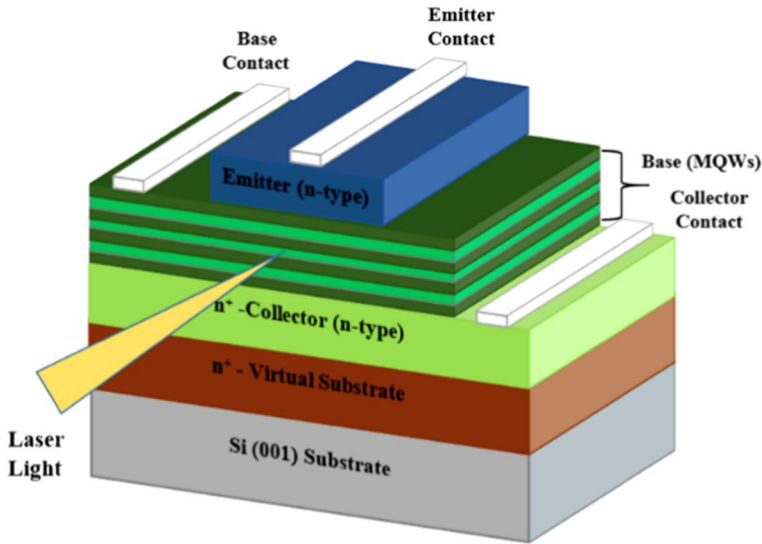
Fig. 1 Schematic of the proposed $Ge_{0.87}Sn_{0.13}/Si_{0.05}Ge_{0.82}Sn_{0.13}$ MQW TL

Table 1 Layers of the structure and their parameters

Layer	Material	Thickness (nm)	Doping (cm^{-3})	Type
Emitter	SiGeSn	150	1×10^{19}	n
Barrier	SiGeSn	16 and 22	1×10^{18}	p
Well	GeSn	12 and 22	–	i
Collector	GeSn	200	1×10^{17}	n
Virtual-Substrate	GeSn	200	–	i
Substrate	Si	400	–	i

2 Proposed $Ge_{0.87}Sn_{0.13}/Si_{0.05}Ge_{0.82}Sn_{0.13}$ MQW TL structure

Figure 1 shows the three-terminal proposed (*n-p-n*) $Ge_{0.87}Sn_{0.13}/Si_{0.05}Ge_{0.82}Sn_{0.13}$ MQW TL structure in layers. GeSn buffer that is fully strain-relaxed (200-nm-thick) is presumed to be grown on the silicon (001) substrate and to act as the virtual substrate (VS) will lead to a reduction of defects and a subsequent increase in QWs. Afterwards, a thick layer of 200 nm is deposited as the collector. On the same buffer, MQWs with three periods of $\{Si_{0.05}Ge_{0.82}Sn_{0.13}/Ge_{0.87}Sn_{0.13}\}$ are grown. All quantum wells in a MQW stack have the same composition and layer thickness. For MQW-A, the well and barrier thicknesses are 22 nm/22 nm and for MQW-B they are 12 nm/16 nm, respectively (Stange et al. 2018). Finally, the structure is capped by an n-type SiGeSn layer, which acts as an emitter. There are various parameters of the structure listed in Table 1 and alloy composition and layer thickness of MQW-A, and MQW-B are included in the Table 2.

Table 2 Alloy composition and layer thickness of the proposed MQW-A, and MQW-B (Stange et al. 2018)

Structure name	Sn content in active layer/QW (%)	Thickness of active layer/QW (nm)	Si/Sn content in barrier (%)	Barrier thickness (nm)
MQW-A	13.3	22	4.8/13.0	22
MQW-B	13.5	12	5.2/13.4	16

3 Theoretical model

3.1 Terminal current

The dc carrier concentrations δN_1 and δN_2 respectively, by solving the time-independent continuity equation for diffusion-dominated transport process with boundary conditions, we can calculate the QW in the base region before and after QW. (Basu et al. 2011)

$$\delta n(z_Q^-) = \delta n\left(z_Q^+\right) = N_{vs} \text{ and } \delta n\left(W_B\right) = 0, \tag{1}$$

and can be expressed as

$$\delta N_1 = \frac{N_{vs} - J_E(L_D/qD_n)e^{-z_Q/L_D}}{2\cosh(z_Q/L_D)}e^{z/L_D} + \frac{N_{vs} + J_E(L_D/qD_n)e^{z_Q/L_D}}{2\cosh(z_Q/L_D)}e^{-z/L_D} \tag{2}$$

$$\delta N_2 = \frac{N_{vs}e^{-W_B/L_D}}{2\sinh(\frac{z_Q-W_B}{L_D})}e^{z/L_D} + \frac{N_{vs}e^{-W_B/L_D}}{2\sinh(\frac{W_B-z_Q}{L_D})}e^{-z/L_D} \tag{3}$$

$$I_E = BN_{vs}\sinh\left(z_1\right) + BN_{vs}\coth\left(z_2\right)\cosh\left(z_1\right) - AJ_{vs}\cosh\left(z_1\right) \tag{4}$$

$$I_C = BN_{vs}\coth\left(z_2\right)\cosh\left(z_2\right) + BN_{vs}\tanh\left(z_2\right)\cosh(z_2) \tag{5}$$

and $I_B = I_E - I_C$ where $B = \frac{A_q D_n}{L_D}$, $z_1 = \frac{z_Q}{L_D}$, $z_2 = \frac{W_B-z_Q}{L_D}$ and A = device's area in total, and

$$J_{vs} = qD_n\left[\frac{d}{dz}\left(\delta N_1\right)_{z=z_Q^-} - \frac{d}{dz}\left(\delta N_2\right)_{z=z_Q^+}\right] \tag{6}$$

3.2 Optical characteristics

The mathematical expression for optical gain in the QW structure is given as (Mukhopadhyay et al. 2018)

$$g(\hbar w) = C_0 \sum_{n,m} \left|I_{hm}^{en}\right|^2 \int_0^\infty dE_t\rho_r^{2D}\left|\hat{e}.p_{cv}\right|^2 \times \frac{\Gamma/2\pi}{\left[E_{hm}^{en}(0) + E_t - \hbar\omega\right]^2 + (\Gamma/2)^2}[f_c^n\left(E_t\right) - f_v^m(E_t)] \tag{7}$$

where $C_0 = \frac{\pi q^2}{n_r c \epsilon_0 m_0^2 \omega} \rho_r^{2D} = \frac{m_r}{\pi \hbar^2 d} I_{hm}^{en} = \int_{-\infty}^\infty dz\phi_n(z)g_m(z)$

$$f_c^n(E_t) = \frac{1}{1 + \exp\{[E_g + E_{en} + (m_r/m_e^*)E_t - F_c]/k_B T\}}$$

$$f_v^m(E_t) = \frac{1}{1 + \exp\{[E_{hm} - (m_r/m_h)E_t - F_v]/k_B T\}}$$

$|\hat{e}.p_{cv}|^2$ is element of the momentum matrix, Γ is the fixed linewidth, m_r is the mass reduction, E_g as a bandgap, F_C and F_V are the Quasi-Fermi levels for electrons and holes, respectively, E_{en} and E_{hm} are the energy of the subbands in conduction and valence bands, respectively, and E_t is the transition energy, T is the temperature.

3.3 Band calculations

The unstrained bandgap of binary and ternary alloy GeSn and SiGeSn can be described as

$$E_{g,\eta}(Ge_{1-p}Sn_p) = (1-p)E_{g,\eta}(Ge) + pE_{g,\eta}(Sn) - p(1-p)b_\eta^{GeSn} \tag{8}$$

$$\begin{aligned} E_{g,\eta}(Ge_{1-x-y}Si_xSn_y) = {} & (1-x-y)E_{g,\eta}(Ge) + xE_{g,\eta}(Si) \\ & + yE_{g,\eta}(Sn) - x(1-x-y)b_\eta^{SiGe} - y(1-x-y)b_\eta^{GeSn} - xyb_\eta^{SiSn} \end{aligned} \tag{9}$$

where b_η^{SiGe}, b_η^{GeSn}, and b_η^{SiSn} are the bowing parameters for the GeSn, SiGe, and SiSn alloys, respectively, and η describes the Γ and L conduction valleys (Chang et al. 2010, 2009).

In order to compare all the band energies, we first find the average valence band energy of SiGeSn-based hetero-structures using the relation

$$E_{V,aV} = -0.48x + 0.69y \tag{10}$$

which sets $E_{V,aV} = 0$ for the pure Ge. As a result of spin–orbit splitting in an alloy, the top of the valence band (heavy and light holes) can be calculated by the following formula:

$$E_V = E_{V,aV} + \frac{\Delta_0}{3} \tag{11}$$

Table 3. provides some calculated parameters used in the simulation of GeSn TL and few of the parametric values of Si, Ge and Sn are given in Table 4.

Table 3 Parameters used in the calculation (Mukhopadhyay et al. 2018)

Parameter	Symbol	Value
Spontaneous emission time	τ_s	15 ns
Capture time	τ_c	0.8 ps
Escape time	τ_e	1.2 ps
Confinement factor	Γ_c	0.07

Table 4 Parameter values of Si, Ge and Sn (Mukhopadhyay et al. 2018)

Parameter	Si	Ge	Sn
m_{eff} (Γ valley)	$0.528 m_o$	$0.037 m_o$	$0.058 m_o$
a (A°)	5.4307	5.6537	6.4892
Δ_o (eV)	0.044	0.30	0.8
E_{gL} (eV)	1.65	0.664	0.092
$E_{g\Gamma}$ (eV)	4.185	0.805	-0.413

4 Results and discussion

We initiated with a strain-relaxed GeSn layer that serves as a collector for lattice-matched SiGeSn base layer. Now, QWs of GeSn material are inserted in the base region. For Type-I direct bandgap QW structure, the appropriate compositions of Si, Ge, and Sn (x, y, and p) have been chosen using Eqs. (8 and 9).

We have chosen the composition of base region (barrier/well/barrier) as $Si_{0.05}Ge_{0.82}Sn_{0.13}/Ge_{0.87}Sn_{0.13}$ with different well widths (12 nm and 22 nm) respectively. The emitter is chosen as SiGeSn to make sure its bandgap is higher than that of the base layer. While selecting the compositions, it is important to ensure the direct band-gap for all layers, as well as a reasonably high value for band-offsets at the hetero-junctions and between the barriers and wells at the base.

4.1 Factors that affect threshold base current with QW width

The threshold current density can be calculated using this equation

$$J_{th} = J_{tr} + \left[\frac{qd}{\Gamma c\eta a\tau_s} \right] \cdot [\alpha + \alpha_m] \tag{12}$$

where, $J_{tr} = qdN_{tr}/\tau_s$, $\alpha m = \left(\frac{1}{2L} \right)\ln\left(\frac{1}{R1R2} \right)$, τ_s is the spontaneous emission lifetime (15 ns), Γ_c is the factor of optical confinement, η is the internal quantum efficiency (0.8), α is the coefficient of loss, L is the length of device, R1 and R2 are the reflectivity of the mirrors on the front and back respectively (Fig. 2).

The lasing threshold current J_{th} is used to calculate the required density of virtual current J_{vs} and density of virtual carriers Nvs using the equation

$$\frac{J_{vs}}{q_d} = \frac{J_{qw}}{q_d} - \frac{N_{vs}}{\tau_s} \text{ and } \frac{J_{qw}}{q_d} = \frac{N_{vs}}{\tau_{cap}} - \frac{N_{qw}}{\tau_{esc}} \tag{13}$$

Based on the virtual current density and virtual carrier density, Eqs. (2) and (3) were used to calculate the threshold value of the base current.

In Fig. 3, we present the estimated threshold base currents when the quantum well is positioned at different locations (39, 59, and 79 nm) in the base region for different quantum well widths (12, 16, and 22 nm). When the quantum well is positioned at the center of the base region (59 nm), the threshold base current is 1.133 mA for quantum well width = 22 nm, which is much lower than the values reported for TLs of GeSn and InGaAs.

It is obvious from the Fig. 3 that the increased threshold base current is due to the quantum wells approaches to collector base junction. Current density in the virtual state (Jvs) is

Fig. 2 MQW-A and MQW-B Structure of well width 22 and 12 nm

Fig. 3 Comparison of threshold base current **a** well width = 22 nm (MQW-A) structure **b** well width = 12 nm (MQW-B) structure
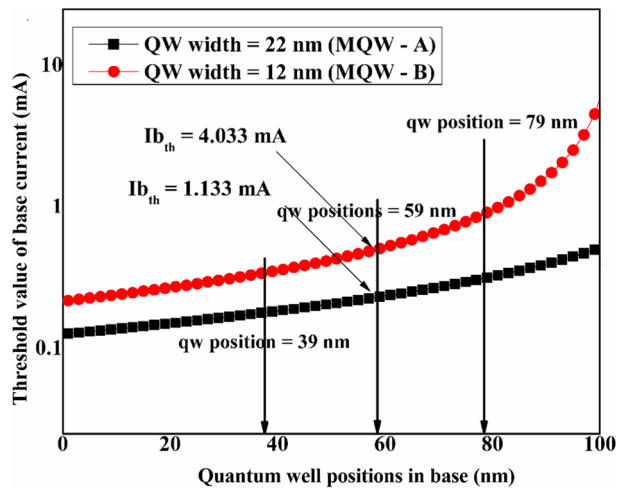

amount corresponding to the difference between two slopes of carrier distribution before and after QW. This difference decreases as the QW approaches the collector–base junction, resulting in a higher injection to maintain the same virtual state current density, again increasing the threshold value for the base current.

There is no experimental data for GeSn TL (threshold base current) in the literature as of yet. Therefore, comparisons have been made between the estimated threshold base current values with the currently available theoretical values of GeSn TL and some of the experimental values of InGaAs TL. Figure 3 clearly depicts that the smaller threshold current value can be obtained by comparing to our earlier work based on GeSn TL (Mukhopadhyay et al. 2018) and theoretical and experimental values of InGaAs TL (Feng et al. 2007, 2006; Then et al. 2010). It may be pointed out that, as emission wavelength, and capture and escape time are different for GeSn based TL from the corresponding values in InGaAs TL, no meaningful comparative analysis is, therefore, possible. Therefore, we may only conclude that the compared direct bandgap GeSn using TL performs better and

Table 5 Comparative study of $Ge_{0.87}Sn_{0.13}/Si_{0.05}Ge_{0.82}Sn_{0.13}$ MQW TL and InGaAs MQW TL performance of threshold base current with different QW width (12, 16, 22 nm)

MQW				SQW					
Proposed Structure $Ge_{0.87}Sn_{0.13}/Si_{0.05}Ge_{0.82}Sn_{0.13}$ MQW TL		GeSn TL Basu et al. 2019) Theoretical		GeSn TL Mukhopadhyay et al. 2018) Theoretical		InGaAs TL Basu et al. 2011) Theoretical		InGaAs TL Feng et al. 2004b; Feng et al. 2007; Then et al. 2010; Feng et al. 2006) Experimental	
Well width (nm)	Ib_{th} (mA)	Well width (nm)	Ib_{th} (mA)	Well width (nm)	Ib_{th} (mA)	Well width (nm)	Ib_{th} (mA)	Well width (nm)	Ib_{th} (mA)
12	4.037	12	4.17	12	–	12	3.6	12	40
16	–	16	2.65	16	3.2	16	21.5	16	22
22	1.133	22	–	22	–	22	–	22	-

Fig. 4 Laser-light output power of GeSn TL compared for **a** MQW-A structure (well width 22 nm) **b** MQW-B structure (well width = 12 nm)
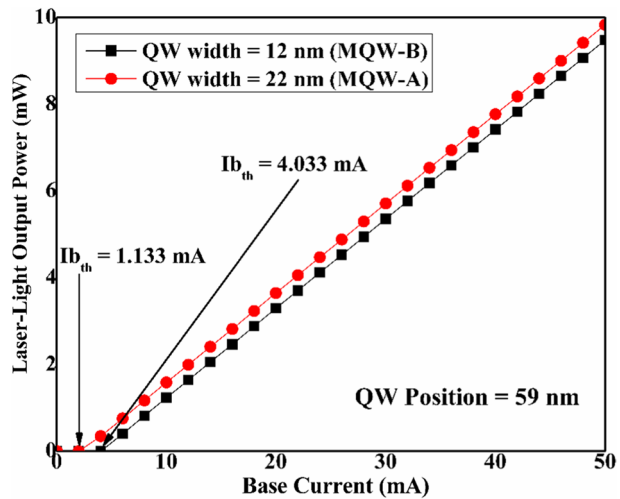
ensures low threshold base current. Table 5 provides the comparative analysis between the $Ge_{0.87}Sn_{0.13}/Si_{0.05}Ge_{0.82}Sn_{0.13}$ and InGaAs MQW TL in terms of threshold base current with different QW widths (12, 16, 22 nm). It may be seen that the proposed GeSn MQW TL structure is capable of providing the threshold base current of ~ 1.133 mA for QW width = 22 nm and ~ 4.037 mA for QW width = 12 nm which is consistently decreases from the previous report values of GeSn and InGaAs-based MQW TLs.

4.2 QW width effects on light output power characteristics (L-I curve)

Figure 4 shows the calculated values of light output laser power for different base current values. The QW positioned at 59 nm away from the emitter–base junction is assumed. Once the threshold base current is reached, the light output power increases abruptly.

The light output power (P) increases linearly as the base current changes according to the given relation:

$$P = \frac{\hbar\omega}{q}\left[\frac{\alpha_m}{\alpha + \alpha_m}\right](IB - IB_{th}) \tag{14}$$

where, α_m is the mirror loss, and the electronic charge is denoted by q.

From Fig. 4, it is clear that the rate of increase of laser light output power is higher in case of QW thickness 22 nm as compared to QW thickness 12 nm This attributes to the lower threshold base current that is obtained in this case.

4.3 Effect of temperature on threshold base current for MQW-A and MQW-B Structure

The estimated value of base current threshold when a quantum well is located at three different locations (39, 59 and 79 nm) in the base region for different quantum well width (22 nm and 12 nm) at different temperatures is refer in Fig. 5. Quantum well threshold current is around 1.133 mA when the quantum well is positioned at the centre of the base region (i.e. 59 nm) for quantum well width 22 nm at a temperature 300 K. which is much lower as compared to the low temperature 4 K. From the above fig., it is clearly seen that the threshold base current increases as temperature approaches to lower value i.e. 4 K.

4.4 Effect of temperature on light output power for MQW-A and MQW-B Structure

From Fig. 6a and b, it is clear that the rate of increase of light output power is maximum at temperature 300 K as compared to temperature 4 K in both the cases with QW thickness 22 nm and 12 nm, respectively. This attributes to the minimum threshold base current achieved at room temperature as compared to temperature 4 K.
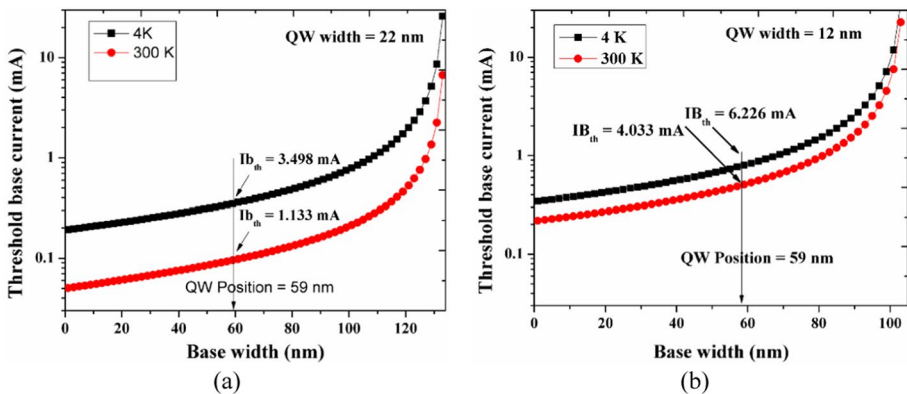

Fig. 5 Comparison of threshold base current for different temperatures 4 K and 300 K **a** well width = 22 nm (MQW-A) structure **b** well width = 12 nm (MQW-B) structure
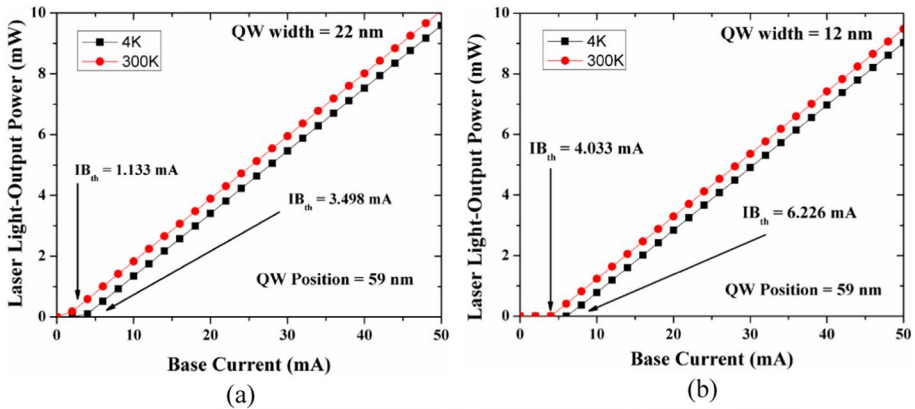
Fig. 6 Comparing laser light output for different temperatures 4 K and 300 K with **a** MQW-A (well width 22 nm) **b** MQW-B (well width = 12 nm)
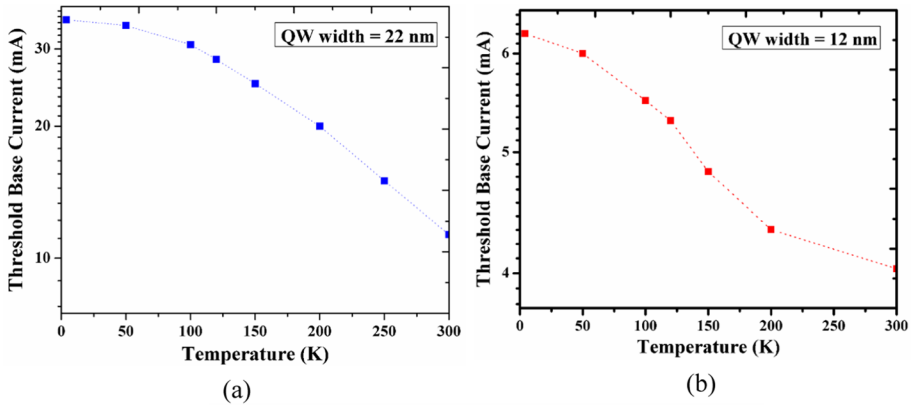

Fig. 7 Shows the threshold base current with the variation of temperature (0 to 300 K) for QW width = 22 nm and 12 nm

Figure 7a and b clearly shows that the threshold base current decreases with the increase of temperature (0 to 300 K) for QW thickness 22 nm and 12 nm. Hence, we conclude that maximum threshold current for base is obtained at low temperature, and minimum threshold value of base current is obtained at room temperature (300 K).

4.5 Effect of QW thickness on injected carrier concentration in base layer

Figure 8 indicates minority carrier distribution along the base region of MQW $Ge_{0.87}Sn_{0.13}$ /$Si_{0.05}Ge_{0.82}Sn_{0.13}$ TL with different QW widths (12, 16, 22 nm). The profiles for three different QW widths for TLs show the same pattern as indicated in Kumar et al. (2018); however, QW width = 22 nm shows a steeper slope indicating higher and more confinement of carriers in the base region as compared to the TL with 12 nm QW width. Steeper slope
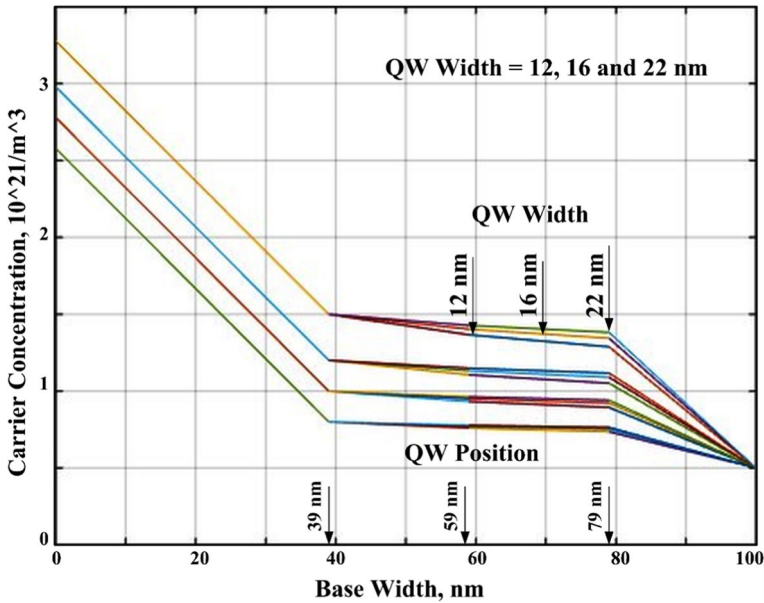
Fig. 8 Variation of current injected in the base when QW is placed at three different positions (39, 59 and 79 nm) for densities of virtual state carriers with different qw width (12,16 and 22 nm)

ensures fast disposal of minority carriers so that fewer carriers wait to recombine and that results in a resonance-free modulation response.

Figure 9 shows the optical modulation BW of $Ge_{0.87}Sn_{0.13}/Si_{0.05}Ge_{0.82}Sn_{0.13}$ MQW TL. Now, it may be interesting to compare the optical modulation BW of the proposed $Ge_{0.87}Sn_{0.13}/Si_{0.05}Ge_{0.82}Sn_{0.13}$ MQW based TL with the already existing GeSn and InGaAs using MQW TL. Table 6. provides the comparative analysis of optical modulation BW. Figure 9 clearly indicate that, the proposed $Ge_{0.87}Sn_{0.13}/Si_{0.05}Ge_{0.82}Sn_{0.13}$ MQW

Fig. 9 Small signal modulation BW of $Ge_{0.87}Sn_{0.13}/Si_{0.05}Ge_{0.82}Sn_{0.13}$ based MQW TL
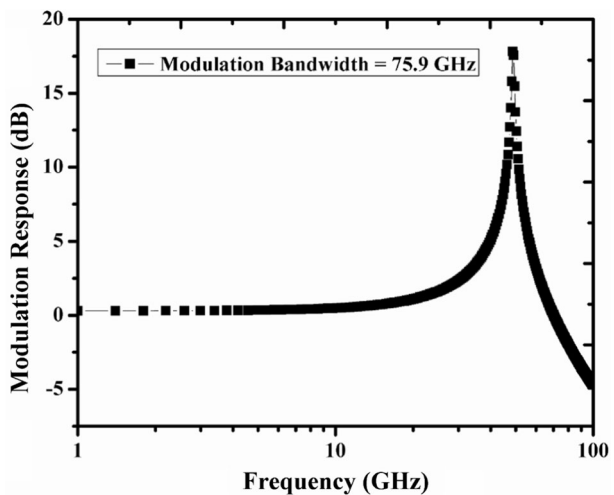
Table 6 Comparison for modulation BW of $Ge_{0.87}Sn_{0.13}/Si_{0.05}Ge_{0.82}Sn_{0.13}$ MQW TL of InGaAs and GeSn material

$Ge_{0.87}Sn_{0.13}$ /$Si_{0.05}Ge_{0.82}Sn_{0.13}$ (Proposed Structure)	GeSn TL (Theoretical) Basu et al. 2019)	InGaAs TL (Theoretical) Kumar et al. 2018)	InGaAs TL (Theoretical) Basu et al. 2012a)	InGaAs TL (Experimental) Feng et al. 2006)
Parameter/modulation bandwidth				
75.9 GHz	53 GHz	29 GHz	21 GHz	13.5 GHz

TL is capable of providing ∼ 75.9 GHz of modulation BW, which is much better than the previously reported values for GeSn and InGaAs-based MQW TLs (Basu et al. 2012a, 2019; Kumar et al. 2018). This enhanced modulation response is due to the more carrier confinement in the direct band-gap $Ge_{0.87}Sn_{0.13}/Si_{0.05}Ge_{0.82}Sn_{0.13}$ structures, which increases the switching speed of propose structure.

Figure 10 demonstrates the rate of spontaneous emission density as a result of photon energy. The TE and TM spontaneous emission rate density is obtained into the $Ge_{0.87}Sn_{0.13}/Si_{0.05}Ge_{0.82}Sn_{0.13}$ TL structure as lasing action occurs in the QWs of base region. As shown in the Fig. 10, the spontaneous emission peak is obtained around 0.8 eV photon energy which is calculated by TCAD simulation tool. Thus, the proposed $Ge_{0.87}Sn_{0.13}/Si_{0.05}Ge_{0.82}Sn_{0.13}$ TL structure is useful for mid-infrared applications such as medical surgery, molecular spectroscopy, gas sensing etc.

Figure 11 depicts the electric potential variation from emitter to collector region through the base region in accordance with increase of voltage of base-emitter which is calculated by atlas software. It clearly indicates that the potential along the distance between the emitter and the collector of $Ge_{0.87}Sn_{0.13}/Si_{0.05}Ge_{0.82}Sn_{0.13}$ MQW TL increases as the base-emitter voltage varies from 0.4 to 1 V.

Figure 12 shows the conduction current density in accordance with increase of voltage at base-emitter from 0.4 to 1 V. The conduction current density shows the sharp rising curve in the well region of the $Ge_{0.87}Sn_{0.13}/Si_{0.05}Ge_{0.82}Sn_{0.13}$ TL structure and increases in accordance with increase of base-emitter voltage. This is due to the more carrier confinement in the well region. So, it can be concluded that more current density will be obtained in the quantum well region of structure of the $Ge_{0.87}Sn_{0.13}/Si_{0.05}Ge_{0.82}Sn_{0.13}$ TL and increases in accordance with increase of voltage.

In Fig. 13, the optical intensity is shown across the base region of $Ge_{0.87}Sn_{0.13}$ /$Si_{0.05}Ge_{0.82}Sn_{0.13}$ MQW TL. The maximum intensity is achieved in the middle of the base region and tends to decrease as we move outwards. It ensures that QW regions undergo stimulated emission and enables coherent mid-infrared emission once the base current reaches its threshold value.

4.6 Effect of temperature on capture and escape time within the QW

Figure 14 shows the escape and capture time with the variation of QW width of GeSn TL at different temperatures. As seen in fig., if we increase the QW width, both escape and capture time increases at low temperature (4 K) and room temperature (300 K), respectively. However, the escape and capture time within the QWs of $Ge_{0.87}Sn_{0.13}/Si_{0.05}Ge_{0.82}Sn_{0.13}$ TLs is very much less at room temperature as compared to low temperature. So, we prefer

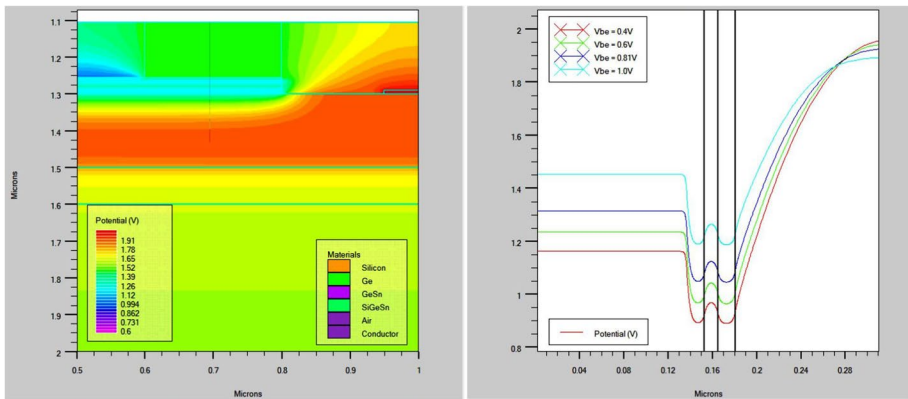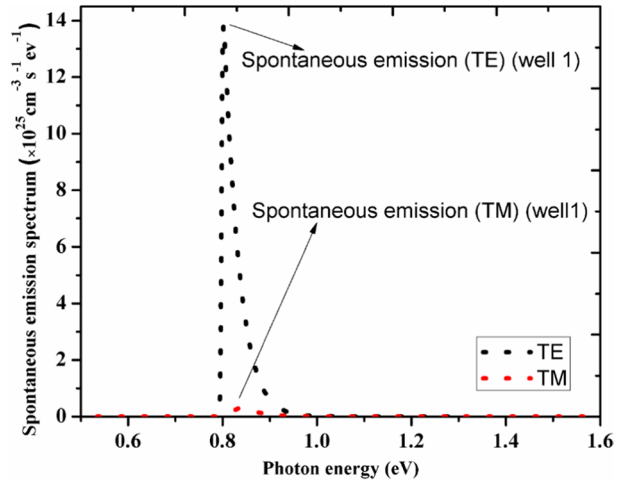**Fig. 10** The spontaneous emission rate density varies with photon energy

Fig. 11 Electric potential variation with the increase of different base-emitter voltages (V_{BE}) (for Sn = 13%, doping of base $1 \times 10^{18} \text{cm}^{-3}$)

the $Ge_{0.87}Sn_{0.13}/Si_{0.05}Ge_{0.82}Sn_{0.13}$ TL operation at room temperature to increase the speed of TL.

5 Conclusion

In our study, we investigated the effect of varying quantum well thickness and temperature on threshold base currents, terminal currents, light output power, and modulation bandwidth of TLs with $Ge_{0.87}Sn_{0.13}/Si_{0.05}Ge_{0.82}Sn_{0.13}$ MQW in the base. Moreover, various simulated characteristics such as spontaneous emission rate density, potential variation, conduction current density, optical intensity etc. also have been studied using TCAD software. Based on the results of the experiments, the laser light output power is a function of base
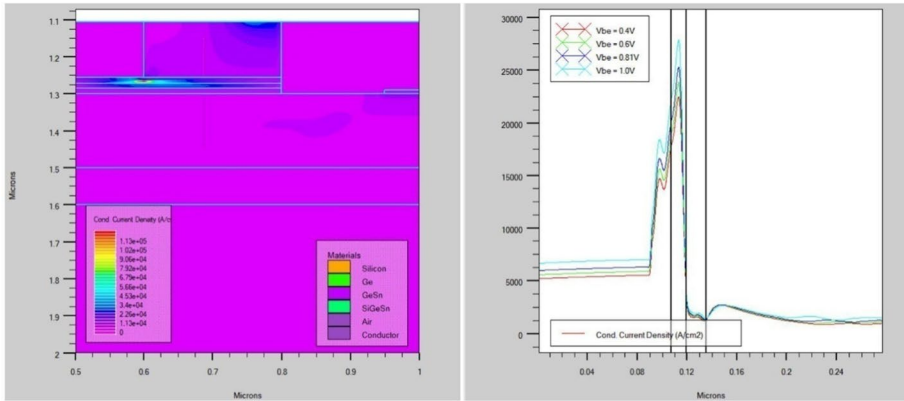
Fig. 12 Conduction current density with the increase of different base-emitter voltages (V_{BE}) (for Sn = 13%, doping of base 1×10^{18}cm^{-3})

current, and the width of the quantum well as well as temperature strongly affect threshold base current. Calculated threshold base current at its lowest value ∼ 1.133 mA, and higher value of modulation BW ∼ 75.9 GHz shows that the proposed structure operates with high speed. This will give encouragement to the workers for the characterization and fabrication of the practical device structure using group IV alloy.
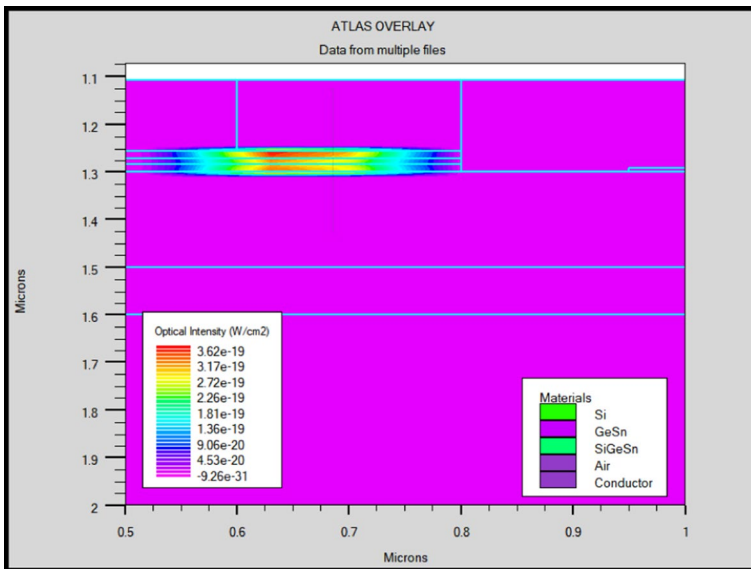
Fig. 13 A cross-sectional view of optical intensity of Ge$_{0.87}$Sn$_{0.13}$/Si$_{0.05}$Ge$_{0.82}$Sn$_{0.13}$ MQW TL
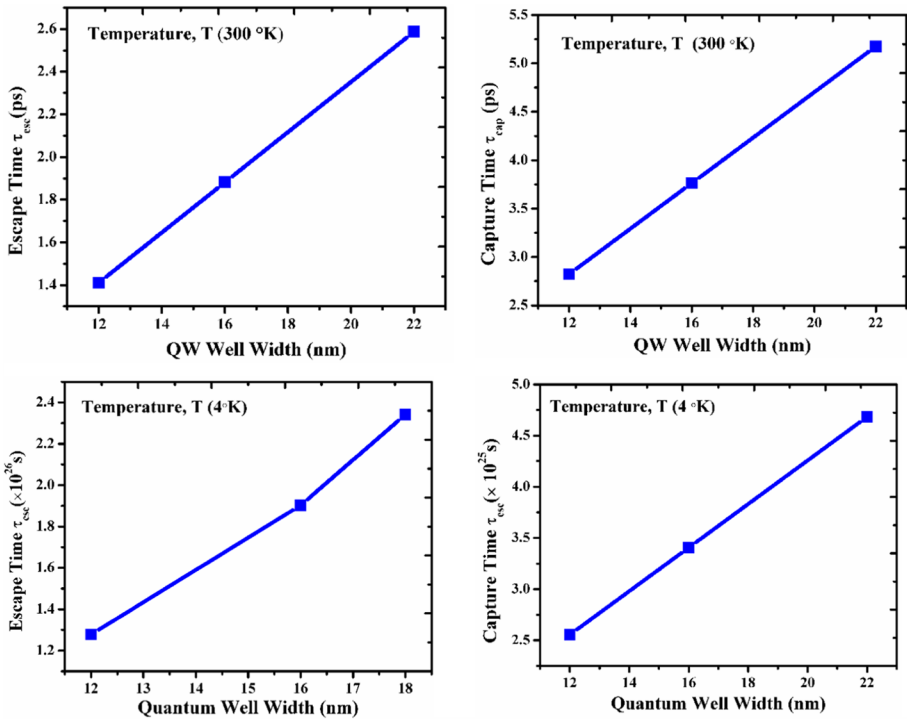
Fig. 14 Escape and Capture time with the variation of QW width at temperature (300 ºK) and (4 ºK)

Author contributions JK did the simulations, prepare results and wrote the manuscript, RB and AKS corrected the manuscript.

Availability of data and materials Not applicable.

Declarations

Conflict of interest The authors declare no competing interests.

Ethical approval Not applicable.

References

Basu, R., Mukhopadhyay, B., Basu, P.K.: Estimated threshold base current and light power output of a transistor laser with InGaAs quantum well in GaAs base. Semicond. Sci. Technol. **26**(10), 105014 (2011)

Basu, R., Mukhopadhyay, B., Basu, P.K.: Modeling resonance-free modulation response in transistor lasers with single and multiple quantum wells in the base. IEEE Photonics J. **4**(5), 1571–1581 (2012a)

Basu, R., Mukhopadhyay, B., Basu, P.K.: Modeling of current gain compression in common emitter mode of a transistor laser above threshold base current. J. Appl. Phys. **111**(8), 083103 (2012b)

Basu, P.K., Mukhopadhyay, B., Basu, R.: Analytical model for threshold-base current of a transistor laser with multiple quantum wells in the base. IET Optoelectron. **7**(3), 71–76 (2013)

Basu, P.K., Mukhopadhyay, B., Basu, R.: Semiconductor Laser Theory. CRC Press, Boca Raton, USA (2015a)

Basu, R., Chakraborty, V., Mukhopadhyay, B., Basu, P.K.: Predicted performance of Ge/GeSn hetero-phototransistors on Si substrate at 1.55 µm. Opt. Quantum Electr. **47**, 387–399 (2015b)

Basu, R., Kaur, J., Sharma, K.: Analysis of a direct-bandgap GeSn-based MQW transistor laser for mid-infrared applications. J. Electr. Mater. **43**, 6335 (2019)

Chang, G.-E., Chang, S.-W., Chuang, S.L.: Theory for n-type doped, tensile-strained Ge–Si_xGe_ySn_1−x−y quantum-well lasers at telecom wavelength. Opt. Express **17**(14), 11246 (2009)

Chang, G.-E., Chang, S.-W., Chuang, S.L.: Strain-balanced GezSn1−z–SixGeySn1−x−y multiple-quantum-well lasers. IEEE J. Quantum Electron. **46**(12), 1813–1820 (2010)

Chang, G., Basu, R., Mukhopadhyay, B.: Design and modeling of GeSn/Ge based heterojunction phototransistors for communication applications. IEEE J. Sel. Top. Quantum Electr. **22**(6), 425–433 (2016)

Faraji, B., Member, S., Shi, W., Fellow, D.L.P.: Analytical modelling of the transistor laser. IEEE J. Select. Topics Quantum Electr. **15**(3), 1–10 (2009)

Feng, M., Holonyak, N., Hafez, W.: Light-emitting transistor: Light emission from InGaP/GaAs heterojunction bipolar transistors. Appl. Phys. Lett. **84**(1), 151–153 (2004a)

Feng, M., Holonyak, N., Chan, R.: Quantum-well-base heterojunction bipolar light-emitting transistor. Appl. Phys. Lett. **84**(11), 1952–1954 (2004b)

Feng, M., Holonyak, N., James, A., Cimino, K., Walter, G., Chan, R.: Carrier lifetime and modulation bandwidth of a quantum well AlGaAs/InGaP/GaAs/InGaAs transistor laser. Appl. Phys. Lett. **89**(11), 1–4 (2006)

Feng, M., Holonyak, N., Then, H.W., Walter, G.: Charge control analysis of transistor laser operation. Appl. Phys. Lett. **91**(5), 10–13 (2007)

Hossain, M.M., et al.: Low-noise speed-optimized large area CMOS avalanche photodetector for visible light communication. J. Lightwave Technol. **35**(11), 2315–2324 (2017)

Kumar, N., Mukhopadhyay, B., Basu, R.: Tunnel injection transistor laser for optical interconnects. Opt. Quant. Electron. **50**(3), 1–12 (2018)

Miller, D.A.B.: Rationale and challenges for optical interconnects to electronic chips. Proc. IEEE **88**(6), 728–749 (2000)

Mukhopadhyay, B., Sen, G., De, S., Basu, R., Chakraborty, V., Basu, P.K.: Calculated characteristics of a transistor laser using alloys of Gr-IV elements. Phys. Status Solidi B **255**(9), 1800117 (2018). https://doi.org/10.1002/pssb.201800117

Oheme, M., Al, E.: GeSn p-i-n detectors integrated on Si with up to 4% Sn'". Appl. Phys. **101**(14), 2–6 (2012)

Pandey, A.K., Basu, R., Chang, G.E.: Optimized Ge1-xSnx/Ge multiple- quantum- well heterojunction phototransistors for high - performance SWIR photodetection. IEEE Sens. J. **18**(14), 5842–5852 (2018)

Ranjan, R., Das, M.K.: Theoretical estimation of optical gain in Tin-incorporated group IV alloy based transistor laser. Opt. Quant. Electron. **48**(3), 1–11 (2016)

Stange, D., et al.: GeSn/SiGeSn heterostructure and multi quantum well lasers. ACS Photonics **5**(11), 4628–4636 (2018)

Taghavi, I., Kaatuzian, H., Leburton, J.P.: Multiple versus single quantum well transistor laser performances. In: Integrated Photonics Research, Silicon and Nanophotonics, pp. 5–7 (2012)

Then, H.W., Feng, M., Holonyak, N.: Microwave circuit model of the three-port transistor laser. J. Appl. Phys. **107**(9), 094509 (2010)

Wirths, S., Geiger, R., et al.: Lasing in direct bandgap GeSn alloy grown on Si (001). Nat. Photonics **9**(2), 88–92 (2015)